International Journal of Computing and Optimization
Vol. 3, 2016, no. 1, 141 - 151
HIKARI Ltd, www.m-hikari.com
https://doi.org/10.12988/ijco.2016.61021

Dilated Capillaries Detection in Dermatoscopic Images

B. Luna-Benoso

Instituto Politécnico Nacional, Escuela Superior de Cómputo, Av. Juan de Dios Batíz, esq. Miguel Othón de Mendizábal, México City 07738, México

J. C. Martínez-Perales

Instituto Politécnico Nacional, Escuela Superior de Cómputo, Av. Juan de Dios Batíz, esq. Miguel Othón de Mendizábal, México City 07738, México

M. Escorza Valles

Instituto Politécnico Nacional, Escuela Superior de Cómputo, Av. Juan de Dios Batíz, esq. Miguel Othón de Mendizábal, México City 07738, México

Abstract

Basal Cell Carcinoma (BCC) also called non-melanoma skin cancer is the type of skin cancer more frequently in people. Usually it occurs in areas exposed to the sun as the face, head, arms and hands without discarding other parts of the body as the nipple, groin and armpit among others. The BCC is a malignant tumor that appears on the skin, is more common than carcinoma squamous cell or melanoma. The BCC grows slowly, producing rarely metastasis but has a local destructive capacity and committed extensive tissue areas, cartilage and rarely bone, mainly damaged the nose and face. Most BCC are unpigmented, so that one of the main criteria for diagnosis, is the identification of blood vessels. Telangiectasia or dilated capillaries are blood vessels most often in the BCC, it is for this reason that in this work presents a methodology for detection dilated capillaries in dermatoscopic images of areas with CBC is presented.

Keywords: Image analysis, image segmentation, basal cell carcinoma, dermatoscopy

1 Introduction

The BCC is the type of skin cancer more often, representing 70% of all types of skin cancer non melanoma, appearing mainly on sun-exposed areas such as arms, face and hands [1, 2, 3]. The CBC is the development of a malignant tumor in the skin and growing slowly, rarely it produces metastasizes, but has a local destructive capacity and affect different areas of tissue, cartilage and bone rarely [4]. The BCC clinical diagnosis is through observation, however, often feel super surface with the intention of identify BCC lesions in their initial stages, you can also perform imaging studies such as computed axial tomography and magnetic resonance to determine the extension on affected areas. The BCC is classified into three types Clinical: morpheaform, superficial and nodular [5, 6, 7]. The morpheaform is the most aggressive form of the BCC, presents injuries coloration on off-white and pink, fuzzy edges and sometimes hard. These lesions infiltrate depth and often go unnoticed [8]. The superficial is in the form of plates larger size and less relief, with pink and reddish coloration or pigmented areas, its growth is slow [9]. The nodular is a small tumor eruptive skin color, hemispherical covered by enlarged blood vessels and scattered. Clinically it is seen solely as a tumor pearly. It occurs most often on the scalp, neck and shoulders, is common central ulceration and tend to heal [10]. Most of the BCC are not pigmented, so one of the main criteria for diagnosis is the identification of blood vessels, specifically dilated capillaries or aboriformes telangiectasia. Telangiectasia are small areas of dilated veins with bright reddish color and with sharp edges [11].

Dermoscopy is a technique often used for clinical diagnosis of the BCC, which, by an optical instrument called dermatoscopy, the image of the lesion is amplified to analyze below the cutaneous surface. Dermoscopy allows visualization of morphological structures through the epidermis, and identifies significant changes in its structure that might indicate malignant appearance in its initial stage [12].

This paper describes the methodology that leads to detection of dilated capillaries or telangiectasia images of areas that presents BCC, this is done by analyzing images dermatoscopic using methods in the spatial domain, where the segmentation is obtained on the dilated capillaries.

2 Proposed Method

2.1 Digital Image

Before entering in detail with the proposed method, it is necessary to mention the definition of what a digital image is. A digital image is a two dimensional function $f(x, y)$ of the light intensity (brightness) in a point in space, where (x, y) coordinates of that point considering the origin at the top left of the image [13]. Since a digital image is a function $f(x, y)$ discretized in both spatial coordinates and in brightness, often as a two-dimensional usually represented matrix $F_{ij} = (f_{ij})_{H\times W}$, where H and W represent the size of the image (H and W referring to height and width of the image respectively) with $f_{ij} = f(x_i, x_j)$ (Figure 1).

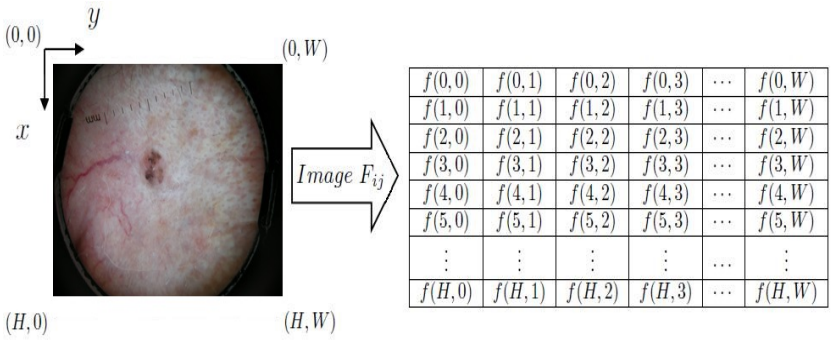

Fig. 1: Digital image.

Given a Dermoscopic image of an affected area by the BCC, the aim of this work is to obtain dilated capillaries, that is, segment the image. An image segmentation involve removing common properties or characteristics of any region of interest. In the case of this paper, the segmentation allows us to obtain dilated capillaries in the dermoscopic images.

Figure 2 shows the dermoscopic image of an affected zone by BCC nodular type, it is noted that the image presents dilated capillaries or telangiectasia.

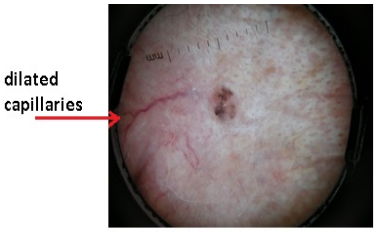

Fig. 2: Dermoscopic image of an area affected by the CBC.

Immediately is presented the algorithm for obtaining the segmentation of dilated capillaries of a dermoscopic image, for this, the algorithm was divided in 5 steps.

Step 1: Given a dermoscopic color image as shown in Figure 2, it decomposes into three levels: Red, Green and Blue (RGB). With the purpose of obtaining an image with the least amount of noise that is applied to the equation 1 using the red and green planes.

$$f(x,y) = (f_R(x,y) - f_G(x,y)) \times 2 - f_G(x,y) \qquad \text{eq. 1.}$$

where f_R and f_G are the appropriate roles of the red and green planes respectively of the color image. Figure 3-a) shows the green plane grayscale and Figure 3-b) shows the red plane grayscale of the image shown in Figure 2. Figure 4-a) shows the result of applying the function on $f_R(x,y) - f_G(x,y)$, Figure 4-b) shows the results of applying the function $((f_R(x,y) - f_G(x,y)) \times 2$ and Figure 4-c) shows the result of applying the equation 1, each one respectively to the images of Figure 3.

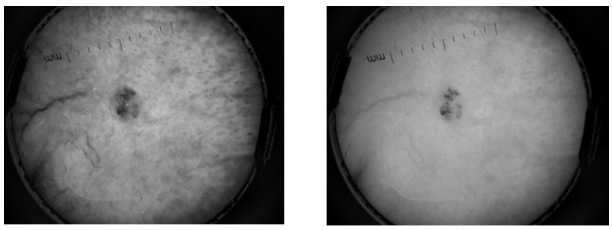

Fig. 3: a) Green plane grayscale, and b) Red plane grayscale.

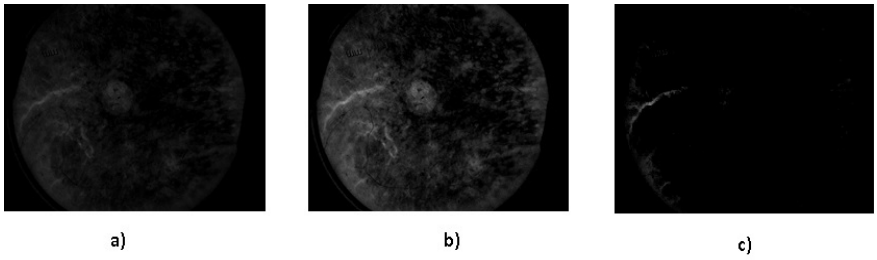

Fig. 4: Result of applying equation 1.

Step 2: Later, the images obtained as in Figure 4, the equation 2 is applied and it is binarized by the equation 3 with u threshold.

$$f(x,y) = \frac{255 * f(x,y)^3}{v_{max}^3 - v_{min}^3} \qquad \text{eq. 2}$$

where v_{max} and v_{min} are the maximum and minimum value of the color image pixels.

$$f(x,y) = \begin{cases} 0 & \text{if} \quad f(x,y) \leq u \\ 255 & \text{in another case} \end{cases}$$

eq. 3

Figure 5 shows the result of applying the equation 2 and 3 to Figure 4.

Fig. 5: Result applying equation 2 and 3.

Step 3: Once binarized the image, related components are extracted and those components are removed with a value of area not within a range, that is, if the A area component related is such that the condition does not meet $a \leq A \leq b$ con a y b two fixed thresholds, then the connected component is eliminated. Figure 6 shows the result of sticking with those connected components that falling within the range $[a, b]$ with a = 80 and b = 5000 to the result of Figure 5.

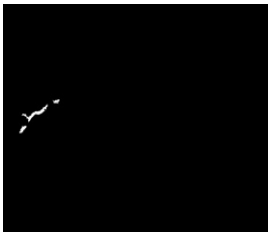

Fig. 6: Related components whose area meet $a \leq A \leq b$.

Figures 7-b) and 7-d) show the result of applying steps 1, 2 and 3 to dermatoscopic images displayed on 7-a) and 7-c) respectively. It is noted that these images have not managed to eliminate noise entirely, so we continue with a process of skeletonization.

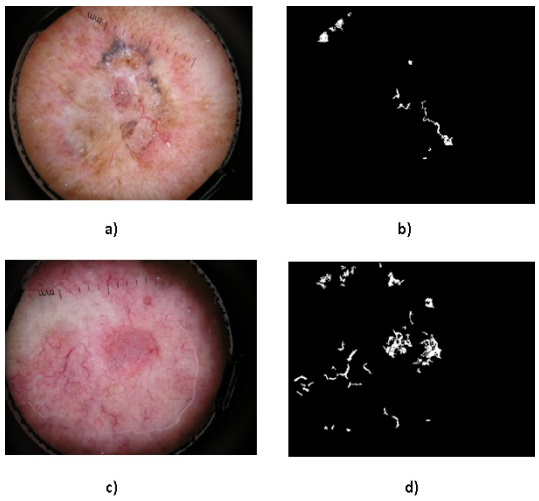

Fig. 7: Result of applying steps 1, 2 and 3 of the algorithm to dermatoscopic images.

Step 4: Zhan-Suen algorithm [14] was applied for obtain the skeletonization of the image obtained in step 3. Figures 8-a) and 8-b) show the result of applying the skeletonization using the Zhan-Suen algorithm to figures 7-b) and 7-d) respectively. An image is observed in which some vessels have bifurcations or branches, and in some images cycles are presented, is observed that those images which have a considerable number of cycles not properly represent capillary dilated, so we proceeded to eliminate those things that had cycles.

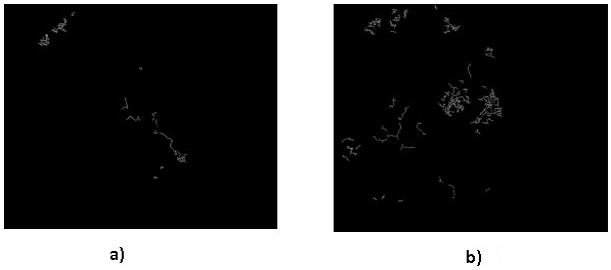

Fig. 8: Images skeletonized by Zhan-Sue.

Step 5: To remove the cycles in the skeletonized image as shown in Figure 8, a structure of FIFO type was used, and a mask of 3×3 was used to look over each of the pixels of the skeleton, such that was analyzed each pixel and those neighboring pixels that had not been look over and that were not adjacent. Figure 9 shows the procedure for finding cycles in the skeleton. Yellow colored pixels represent the pixels already look over, the blue pixels represent the pixels that are being analyzed, the red pixels belonging to the neighborhood of a pixel being analyzed (blue color) but not glued due to the constraint that already glued one adjacent, pixels of green are pixels belonging to a neighborhood of a pixel being analyzed (blue color) and is glued, and pixels purple represent a cycle found. In Figure 9-a) the path of the mask 3×3 is shown, the displayed blue color pixel is analyzed and its immediate neighbor located at the bottom is glued, the pixel analyzed is highlighted in yellow, then the next pixel is removed of the tail (which at this point there is only one) and your neighbor is glued, this procedure continues until find a zone as shown in Figure 9-c) where there are two neighboring pixels but not adjacent of the blue pixel analyzed, so both pixels they glued in order clockwise (in figure 9 are listed pixels of green color in the order as they enter the queue), the pixel is removed to this by leaving the tail and its neighborhood is analyzed by repeating the above procedure until situations occur as shown in Figure 9-i), where two adjacent pixels are glued, so that by analyzing the pixel green with number 1, It shows that in your neighborhood there is a pixel that is already glued (figure 9-j), so it is a cycle (highlighted in yellow in Figure 9-m), and continue with the rest of the skeleton.

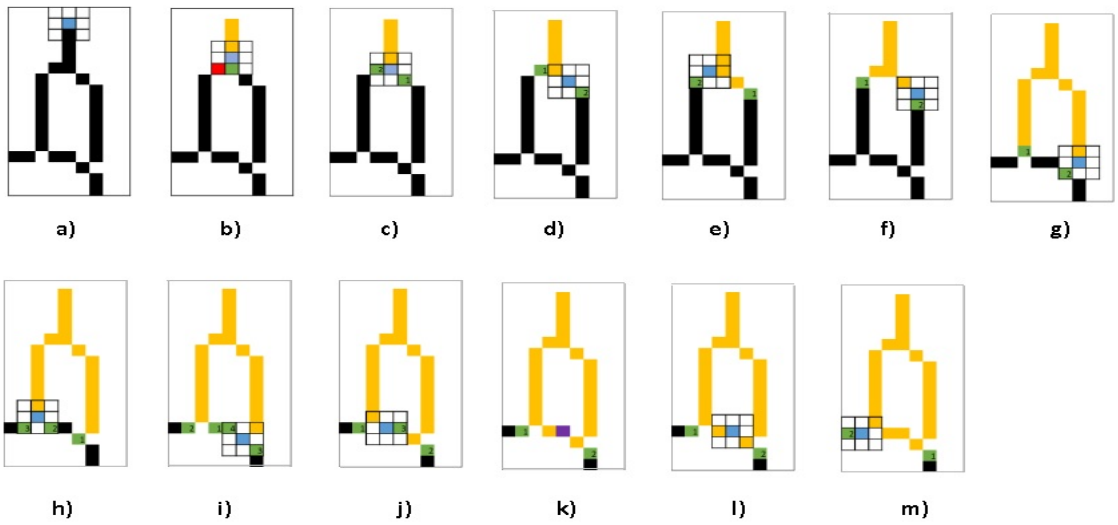

Fig. 9: Location of cycles.

Figures 10-a) and 10-c) show the result of eliminating those areas that containing cycles in the images of Figures 8-a) and 8-b) respectively.

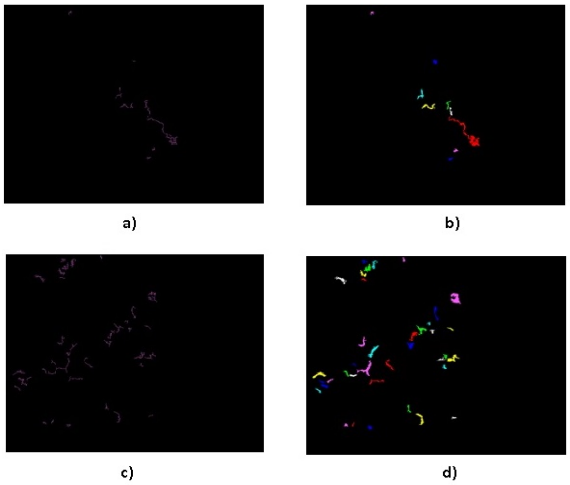

Fig. 10: Elimination of cycles.

Figure 11 shows the result of applying steps 1 to 5 to dermatoscopic figures presented BCC. The areas where the dilated capillaries are located are highlighted in red.

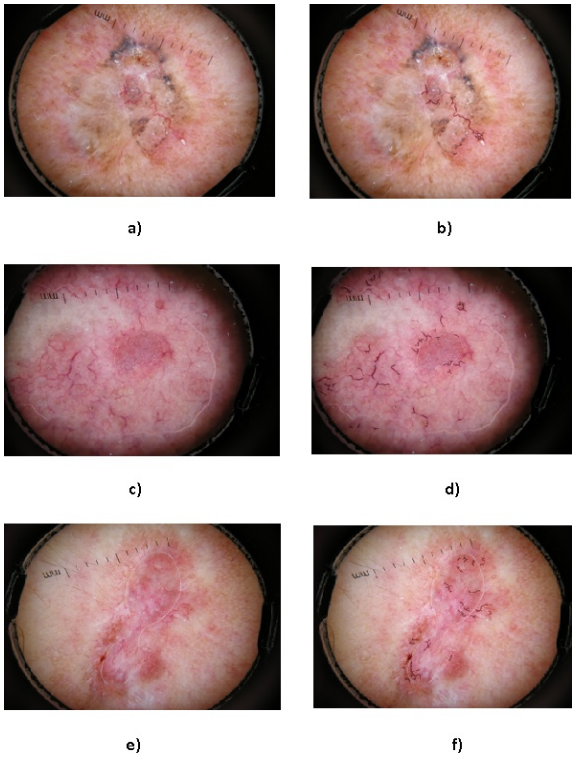

Fig. 11: Location of dilated capillaries.

3 Conclusion

This paper was presented an algorithm that allows the detection of telangiectasias or dilated capillaries in dermoscopic images of patients which have BCC. This was carried out by methods in the spatial domain for this, first the was considered RGB model, where it became a combination of red with green plane by equation 1, 2 and 3, to obtain a binarized image which is observed dilated capillaries blank, however, the images showed noise, so we proceeded to squeletized the image by Zhan-Suen algorithm, and then the cycles were removed that had ramifications, to finally get those areas that had dilated capillaries.

Acknowledgements. The authors would like to thank the Instituto Politécnico Nacional (Secretaría Académica, EDD, EDI, COFAA, SIP, ESCOM and CIDETEC), the CONACyT and SNI for their economical support to develop this work.

References

[1] Navid Noroozi, Ali Zakerolhosseini, Computer assisted diagnosis of basal cell carcinoma using Z-transform features, *Journal of Visual Communication and Image Representation,* **40** (2016), 128-148. https://doi.org/10.1016/j.jvcir.2016.06.014

[2] S. Konopnicki, O. Hermeziu, R. Bosc, I. Abd Alsamad, J.P. Meningaud, Nasal basal cell carcinomas. Can we reduce surgical margins to 3 mm with complete excision?, *Annales de Chirurgie Plastique Esthétique,* **61** (2016), no. 4, 241-247. https://doi.org/10.1016/j.anplas.2016.01.001

[3] Marieke H. Roozeboom, Aimee H.M.M. Arits, et al., Three-Year Follow-Up Results of Photodynamic Therapy vs. Imiquimod vs. Fluorouracil for Treatment of Superficial Basal Cell Carcinoma: A Single-Blind, Noninferiority, Randomized Controlled Trial, *Journal of Investigative Dermatology,* **136** (2016), no. 8, 1568-1574. https://doi.org/10.1016/j.jid.2016.03.043

[4] Karan Saluja, Pulivarthi H. Rao, Jeffery N. Myers, Adel K. El-Naggar, Novel t(1;3)(q21,p21) translocation in a basal cell adenocarcinoma of the parotid gland: potential association with tumorigenesis, *Human Pathology,* **54** (2016), 189-192. https://doi.org/10.1016/j.humpath.2016.03.019

[5] Verena Ahlgrimm-Siess, Michael Horn, Silvia Koller, Ralf Ludwig, Armin Gerger, Rainer Hofmann-Wellenhof, Monitoring efficacy of cryotherapy for superficial basal cell carcinomas with in vivo reflectance confocal microscopy: A preliminary study, *Journal of Dermatological Science,* **53** (2009), no. 1, 60-64. https://doi.org/10.1016/j.jdermsci.2008.08.005

[6] Aimilios Lallas, Thrassivoulos Tzellos, et al., Accuracy of dermoscopic criteria for discriminating superficial from other subtypes of basal cell carcinoma, *Journal of the American Academy of Dermatology*, **70** (2014), no. 2, 303-311. https://doi.org/10.1016/j.jaad.2013.10.003

[7] Abel D. Jarell, Thaddeus W. Mully, Basal cell carcinoma on the ear is more likely to be of an aggressive phenotype in both men and women, *Journal of the American Academy of Dermatology,* **66** (2012), no. 5, 780-784. https://doi.org/10.1016/j.jaad.2011.05.020

[8] Tiago Torres, Virgilio Costa, Using photodynamic therapy in morpheaform basal cell carcinoma to ease surgical treatment, *Journal of the American Academy of Dermatology,* **62** (2010), no. 3, 103. https://doi.org/10.1016/j.jaad.2009.11.407

[9] Taiki Suzuki, Kazumichi Sato, Yoichi Tanaka, Naoshi Nakamura, Tomohiro Yamauchi, Akira Katakura, Nobuo Takano, A case of basal cell carcinoma of the buccal mucosa with black pigmentation, *Journal of Oral and Maxillofacial Surgery, Medicine, and Pathology,* **28** (2016), no. 2, 170-173. https://doi.org/10.1016/j.ajoms.2015.08.005

[10] Joshua Eikenberg, Douglas Grider, Michael Kolodney, Use of clamping to enhance intralesional bleomycin therapy for nodular basal cell carcinoma, *Journal of the American Academy of Dermatology,* **72** (2015), no. 5, 194. https://doi.org/10.1016/j.jaad.2015.02.790

[11] C. Hernandez-Ibanez, M. Aguilar-Bernier, R. Fúnez-Liébana, J. del Boz, N. Blázquez, M. de Troya, The Usefulness of High-Resolution Ultrasound in Detecting Invasive Disease in Recurrent Basal Cell Carcinoma After Nonsurgical Treatment, *Actas Dermo-Sifiliograficas (English Edition),* **105** (2014), no. 10, 935-939. https://doi.org/10.1016/j.adengl.2014.05.021

[12] Fengying Xie, Yang Li, Rusong Meng, Zhiguo Jiang, No-reference hair occlusion assessment for dermoscopy images based on distribution feature, *Computers in Biology and Medicine,* **59** (2015), 106-115. https://doi.org/10.1016/j.compbiomed.2015.01.023

[13] R. González, J. Woods, *Digital Image Processing,* 3rd ed., Prentice Hall, New Jersey, 2008.

[14] T. Y. Zhang, C.Y. Suen, A Fast Parallel Algorithm for Thinning Digital Patterns, *Communications of the ACM,* **27** (1984), no. 3, 236-239. https://doi.org/10.1145/357994.358023

Received: October 18, 2016; Published: November 11, 2016